

## Ultrafast photo-thermal switching of terahertz spin currents

*Piyush Agarwal<sup>#</sup>, Rohit Medwal<sup>#</sup>, Abhishek Kumar, Hironori Asada, Yasuhiro Fukuma, Rajdeep Singh Rawat\*, Marco Battiato\*, and Ranjan Singh\**

P. Agarwal, A. Kumar, Prof. M. Battiato, Prof. R. Singh  
Division of Physics and Applied Physics, School of Physical and Mathematical Sciences,  
Nanyang Technological University, 21 Nanyang Link, Singapore 637371, Singapore  
E-mail: ranjans@ntu.edu.sg

P. Agarwal, A. Kumar, Prof. R. Singh  
Center for Disruptive Photonic Technologies, The Photonics Institute, Nanyang  
Technological University, Singapore 639798, Singapore  
E-mail: ranjans@ntu.edu.sg

Dr. R. Medwal, Prof. R. S. Rawat  
Natural Science and Science Education, National Institute of Education, Nanyang  
Technological University, Singapore 637616, Singapore  
E-mail: rajdeep.rawat@nie.edu.sg

Prof. H. Asada  
Department of Electronic Devices and Engineering, Graduate School of Science and  
Engineering, Yamaguchi University, Ube 755-8611, Japan

Prof. Y. Fukuma  
Department of Physics and Information Technology, Faculty of Computer Science and  
System Engineering, Kyushu Institute of Technology, Iizuka 820-8502, Japan

<sup>#</sup>Equal Contribution

Keywords: Photo-thermal spin switching, terahertz phase reversal, terahertz hysteresis, reconfigurable terahertz emission

Dissipationless and scattering-free spin-based terahertz electronics is the futuristic technology for energy-efficient information processing. Femtosecond light pulse provides an ideal pathway for exciting the ferromagnet out-of-equilibrium, causing ultrafast demagnetization and superdiffusive spin transport at sub-picosecond timescale, giving rise to transient terahertz radiation. Concomitantly, light pulses also deposit thermal energy at short timescales, suggesting the possibility of abrupt change in magnetic anisotropy of the ferromagnet that could cause ultrafast photo-thermal switching of terahertz spin currents. Here, we demonstrate a single light pulse induced photo-thermal switching of the terahertz spin current manifested through the phase reversal of the emitted terahertz photons. The switching of transient spin current is due to the reversal of magnetization state across the energy barrier of the ferromagnetic layer. Our demonstration opens a new paradigm for on-chip spintronic devices enabling ultralow-power hybrid electronics and photonics fueled by the interplay of charge, spin, thermal, and optical signals.

## 1. Introduction

The discovery of laser-induced ultrafast demagnetization<sup>[1]</sup> provides a perfect platform to manipulate spins at sub-picosecond timescales and opens up a promising route to develop future information technology<sup>[2–4]</sup> at terahertz speed<sup>[5,6]</sup>. This intriguing observation revolutionized the field<sup>[7–10]</sup> of terahertz sources by achieving high bandwidth emission at low-cost and highly simplified fabrication approaches<sup>[11,12]</sup>. Typically, these terahertz sources consist of ferromagnet (FM)/heavy metal (HM) heterostructures, where a femtosecond laser pulse excites the spins in the FM layer above the Fermi energy and drives the system out of equilibrium<sup>[1,13–15]</sup>. After the excitation, majority spin carriers<sup>[16,17]</sup> transport more efficiently than minority spin carriers<sup>[16,17]</sup> due to band asymmetry in the FM layer and lead to the injection of spin-polarized current ( $\mathbf{j}_s$ ) from the FM layer to the HM layer through a superdiffusive transport process<sup>[18–20]</sup>. The spins entering the HM layer experience a strong spin-orbit coupling and undergo inverse spin Hall effect (ISHE) to produce a transient transverse charge current ( $\mathbf{j}_c$ ), which emits terahertz radiation. Efficient manipulation of spins and reconfiguration of terahertz waves in spintronic emitters have been so far explored by varying external stimuli such as magnitude and direction of an applied magnetic field<sup>[21,22]</sup>, electric current<sup>[23,24]</sup> or helicity of the incident light pulse<sup>[25]</sup>. Similarly, active manipulation of terahertz radiation has also been demonstrated by replacing the HM layer with Rashba interfaces<sup>[26–28]</sup>, 2DEG<sup>[29]</sup> and topological insulators<sup>[30]</sup>, as a manifestation of high spin orbit coupling.

In this work, we demonstrate single-pulse laser field-induced switching of sub-picosecond terahertz spin current using a photo-thermal effect. Upon laser excitation of a thin FM/HM heterostructure, electrons transition from a strongly out-of-equilibrium to a Fermi-Dirac distribution through an increase in temperature. The time-resolved reflectivity study reveals that the electron system thermalizes with phonons within a few picoseconds, followed by the lateral diffusion of heat throughout the sample surface in tens of picoseconds. This

transient heating from the laser pulse enables control of spin polarization at ultrafast timescale under the presence of a small magnetic field applied opposite to that of the FM magnetization. Ideally, external magnetic fields have been demonstrated to The results also demonstrate that the photo-thermal effect imparted from a single laser pulse is sufficient to change the direction of spin current, which manifests in the form of phase reversal of the emitted terahertz photon. Our results thus unlock a unique approach to realize ultrafast, energy-efficient, single laser pulse induced *photo-thermal switching* (PTS) of spintronics devices.

## 2. Results and Discussions

To illustrate the active control of terahertz spin currents via photo-thermal effect, we chose W/NiFe/Pt samples (**Figure 1(a)**) composed of a permalloy layer ( $\text{Ni}_{80}\text{Fe}_{20}$ , hereon NiFe) in combination with platinum (Pt) and tungsten (W), each having the thickness of 3 nm, on a quartz substrate (refer Supplementary Section S1 and methods for details). Figure 1(b) shows the terahertz pulse after laser irradiation (see methods for details) recorded for the W/NiFe/Pt sample with its spectral bandwidth provided in the inset. Note that the amplitude of the terahertz emission is proportional to charge current  $\mathbf{j}_c$ , where  $\mathbf{j}_c = \gamma \mathbf{j}_s \times \mathbf{M}/|\mathbf{M}|^{[12]}$  with  $\gamma$  as the spin to charge current conversion efficiency,  $\mathbf{M}$  is the magnetization vector of the FM layer, and  $\mathbf{j}_s$  is proportional to the magnetic moment. Additionally, the phase of emitted terahertz radiation can be controlled by manipulating the spin polarization of  $\mathbf{j}_s$  diffusing in the HM layer using an external magnetic field. To investigate the effect of the spin polarization direction, the peak amplitude of the emitted terahertz pulse as a function of an applied magnetic field is recorded, which reveals a Terahertz hysteresis (*THz-H*) behaviour analogous to the *M-H* hysteresis. The obtained *THz-H* hysteresis loop for selected fluences are shown in Figure 1(c), while a comprehensive dataset is provided in Supplementary Section S2. As observed from the figure, we realize that increasing pump laser fluence has a dual effect on the sample, (1) an enhanced

spin current injection from the FM layer to the HM layer, as evident from the increasing terahertz pulse amplitude, and (2) the decrease in the coercive field of the FM layer, which has remained unaccounted for in the previous reports. To elucidate the change in the coercive field with pump fluences, as shown in Figure 1(d), three regions are highlighted as I, II, and III. Region I is characterized as a constant coercivity region, where coercivity does not change with pump fluence of up to  $0.60 \text{ mJ/cm}^2$ . Most of the earlier reported spintronics terahertz emitters operate in region I<sup>[31]</sup>. On the other hand, region II (with laser pump fluence  $> 0.60 \text{ mJ/cm}^2$  and  $\leq 1.05 \text{ mJ/cm}^2$ ) is particularly interesting as the photo-thermal effect starts to induce a reduction in the coercivity of the FM layer without significant change in the amplitude of the emitted terahertz pulse. As the laser pump fluence exceeds  $1.05 \text{ mJ/cm}^2$  (region III), the amplitude of the emitted terahertz and coercive field of the ferromagnetic material remains almost constant with fluence.

Here it is important to highlight that region I reproduce the intrinsic coercive field of the FM as obtained from the M-H hysteresis curve, characterized through vibrating sample magnetometer (VSM) measurements (refer Supplementary Section S2). These results reveal THz-H hysteresis measurement as an ultrafast optical route for investigating magnetic properties such as the coercive field and anisotropy field of the FM layers<sup>[32,33]</sup>. A unified 3D map of pump fluence dependent THz-H hysteresis loop is shown in **Figure 2(a)**. The map is divided into two sections, which illustrates the magnetization switching in the FM layer for the applied magnetic field from 0 Oe to -3 Oe (shown in the left half) and 0 Oe to 3 Oe (right half). The region in red and blue signifies the positive and negative phases of the terahertz pulse, respectively. Here, the terahertz spin currents undergo phase reversal (indicated by the green arrow) by increasing the laser fluence at the applied magnetic field between 0.2 Oe to 2.1 Oe. To probe this effect, we first saturated the sample with a positive magnetic field and applied a negative field of -0.5 Oe (along with the dissect line) insufficient to switch the magnetization direction (Figure 2(b)).

Note that the terahertz pulse amplitude shows an increasing trend with an applied fluence of up to  $0.60 \text{ mJ/cm}^2$  (solid red line) and then gradually diminishes. The emitted terahertz pulse undergoes a complete phase reversal above fluence of  $1 \text{ mJ/cm}^2$ . After switching, a decrease in the laser pump fluence does not restore the original phase of the emitted terahertz pulse (solid black line), indicating the memory effect. However, on the subsequent reversal of the applied magnetic field polarity and an increase in laser fluence can drive the system back to its initial phase. The laser fluence dependent terahertz phase reversal, as shown in Figure 2(b), arises due to an increase in sample temperature, which decreases the energy barrier  $\Delta U(H, T)$  between the two stable magnetization states<sup>[34,35]</sup> and enhances the probability of magnetization switching for a given magnetic energy. Consequently, as pictorially depicted in Figure 2(c), for  $-0.5 \text{ Oe}$ , the thermal energy provided by laser fluence  $0.15 \text{ mJ/cm}^2$  is insufficient for spins to overcome the reduced  $\Delta U$ ; however, a higher laser fluence  $> 1 \text{ mJ/cm}^2$  (Figure 2(d)) provides sufficient thermal energy to switch the magnetization direction of the FM layer along the direction of the applied magnetic field.

Further, to unravel the temporal dynamics of terahertz phase switching in the spintronic heterostructure, the understanding of the following processes become extremely important: (i) the underlying processes of energy flow through the system, (ii) involved time scales of the different processes, and (iii) the shortest timescale at which the photo-thermal energy affects the FM layer magnetization. To address these questions, the transient reflectivity of the sample is measured, as shown in **Figure 3(a)**. The measured ultrafast reflectivity of the W/NiFe/Pt sample for different laser pump fluences allows for an estimation of the electron temperature (refer Supplementary Section S3)<sup>[36,37]</sup>. The reflectivity value at a negative timescale indicates the remnant temperature from the previous laser pulse. This shows (inset of Figure 3(a)) that the optical pulse indeed thermally affects the sample and can control its magnetization and, consequently, the amplitude and the phase of the terahertz pulse, respectively. The fundamental

question is whether this thermal effect is a cumulative effect from all the previous pulses, or is it purely dominated by the previous single pulse? Addressing the question requires a deep understanding of the underlying mechanism. Upon illumination, electrons absorb energy leading to an instantaneous rise in temperature (dotted red line in Figure 3(b)). Within a few picoseconds, the electronic system thermalizes (solid red) with the phonons (solid blue), as shown in Region I of Figure 3(b). As a consequence, the temperature of the illuminated area of the trilayer increases substantially as compared to the other parts of the sample<sup>[36,38]</sup>. Over a timescale of the next hundred picoseconds (region II), fast lateral heat diffusion occurs throughout the metallic trilayer, which decreases the metal temperature in the illuminated region although remains higher than the room temperature. In the last process, as shown in region III, the presence of a high-temperature gradient between the metallic layer and the environment triggers heat transport through the substrate with single exponential decay of the temperature towards room temperature (purple line).

To investigate these photo-thermal effects, we explicitly describe the electronic temperature with the two-temperature (2T) model, which accounts for heat diffusion from electrons and lattice (refer Supplementary Section S3). Note that region III of Figure 3(b) deviates from the 2T model since the model does not account for thermalization with the environment. Moreover, this evidently indicates that heat has been uniformly manifested in the metallic layer in an ultrafast time scale of  $\sim 120$  ps and slowly thermalize with room temperature thereafter. Within this region, the most dominant effect is the heat diffusion through the substrate from a high temperature ( $T_H$ ) towards room temperature ( $T_R$ ) (see the purple line and the inset of Figure 3(b)). Here, the metallic layers have an overall negligible thickness and, therefore, can be described by a single temperature. This is an excellent approximation given the large difference in thickness between metallic layers and substrate. This approximation allows us to treat the

heat flow through the substrate by using Fourier's law to obtain  $Q = -k \frac{T_M(t) - T_R}{\Delta x}$  (refer Supplementary Section S4). Assuming a simple linear relationship between the temperature and metallic layer's internal energy, a decrease in the temperature in those layers due to heat transport through the substrate can be written as

$$\frac{dT_M(t)}{dt} = -A k \frac{T_M(t) - T_R}{C \Delta x}$$

where  $A$  is the sample area, and  $C$  is the effective metallic layer's heat capacity. By knowing the temperature  $T_H$  that the metallic layers have at the beginning of Region III, we can write the temperature after a given time as

$$T(t) = T_R + (T_H - T_R)e^{-k A t / C \Delta x}$$

The temperature  $T_n(t)$  decreases with time  $t$  (from the time at which the  $n$ -th pulse hits the system) is given as,

$$T_n(t) = T_R + (T_{H,n} - T_R)e^{-k A t / C \Delta x}$$

Assuming the incident power of the laser pulse is  $P$ , the increase in the temperature of the metallic layers after the  $n$ -th pulse can be written as  $T_{H,n} - T_{0,n} = P/C$  where  $T_{H,n}$  is the temperature right after the sample achieves a uniform lateral temperature and  $T_{0,n}$  is the temperature of the system right before the  $n$ -th laser pulse illuminates it. Let us highlight again that  $T_{0,n}$  is not room temperature but will depend on the previous excitation(s) through  $T_{0,n} = T_{n-1}(\tau)$ . We can, therefore, obtain the recursive equation that links the power of the  $n$ -th pulse to the temperature of the system right before it is illuminated by the subsequent pulse:

$$T_{0,n+1} = T_R + \left(T_{0,n} + \frac{P}{C} - T_R\right) \lambda; \quad T_{0,1} = T_R.$$

where  $\lambda = e^{-k A \tau / C \Delta x}$  is the temperature loss factor, and  $\tau$  is the laser repetition time. The equation above links the temperature of the sample when it is irradiated by  $(n + 1)$ -th pulse.

The temperature  $T_{0,n}$  reaches a steady-state value of  $T_R + \frac{P \lambda}{C - \lambda C}$  after a number of pulses of the



order of  $1/\lambda$ . So, on assuming that the first pulse hit the system when it was at room temperature, the temperature of the system right before the second and third pulse is

$$T_{0,2} = T_R + \frac{P_1}{C} \lambda, T_{0,3} = T_R + \frac{P_2}{C} \lambda + \frac{P_1}{C} \lambda^2$$

To make sure that pulse #1 can tune the response from pulse #2, the second term in the sum above needs to be sizeable. Experimental values from the exponential decay from region III in Figure 3(b) allows us to estimate the loss factor  $\lambda = \frac{T_0 - T_R}{T_H - T_R} = \frac{361 - 300}{600 - 300} \sim 0.20$ . We, therefore, obtain  $\lambda^2 \sim 0.04$ . This reveals that, at each instance of terahertz emission, the remnant heat in the system is mainly contributed ( $\sim 83\%$ ) by the immediate previous laser pulse. Hence, the experimental data largely free from heat accumulation from multiple pulses evidently proves that a single laser pulse can be employed to exhibit the photo-thermal effect and its manifestation in 120 ps highlights the potential for ultrafast data processing speeds.

Conclusively, in order to experimentally verify the validity of photo-thermal switching just from the preceding laser pulse, we designed a terahertz setup (Figure 4(a)) to illuminate the spintronic emitter with two temporally separated laser pulses. The fluences of the two laser pulses were chosen from region I and region II (Figure 1d) as  $0.15 \text{ mJ/cm}^2$  and  $0.90 \text{ mJ/cm}^2$ . Figure 4(b) shows the terahertz emission from two laser pulses #1 & #2 at time instances of  $t_1$  and  $t_2$  ( $t_2 = t_1 + 1.3 \text{ ns}$ ), respectively. Using these temporally separated pulses, we investigate the sample for three different scenarios, as shown in Figure 4. In Figure 4(c), the laser pulse at time instance  $t_1$  illuminates the sample with a low fluence of  $0.15 \text{ mJ/cm}^2$ , while the pulse at  $t_2$  is switched off. The behaviour shows a THz-H hysteresis loop at time instance  $t_1$  with an unchanged coercive field of  $\sim 2.0 \text{ Oe}$ . In the second case (Figure 4(d)), the sample is illuminated with a high fluence of  $0.90 \text{ mJ/cm}^2$ , which shows a reduction in the coercive field from  $2.0 \text{ Oe}$

to 0.9 Oe as observed in the THz-H loop measured at time  $t_1$ . Finally, in Figure 4(e), both laser pulses, #1 at time  $t_1$  (0.15 mJ/cm<sup>2</sup>) and #2 at time  $t_2$  (0.90 mJ/cm<sup>2</sup>), illuminate the sample in such a way that pulse #1 is always preceded by pulse #2. Remarkably, although the THz-H hysteresis loop was observed at time instance  $t_1$  when low fluence laser pulse was applied, the hysteresis shows reduced coercivity response similar to that in Figure 4(d), as if the THz hysteresis was being observed under high laser fluence. This observation provides the clinching evidence for the occurrence of the ultrafast photo-thermal switching effect.

The decreased coercivity measured at the time instance  $t_1$  of low-fluence pulse #1 experimentally validates that indeed the photo-thermal effect in the system was induced by the preceding high-fluence pulse #2, which modified the spin-population in the system. Further, it is important to note that the photo-thermal effect from a single laser pulse causes the spin reconfiguration in an ultrashort timescale of 120 ps, corresponding to a data processing speed of ~10 GHz, which is three times higher than the current state of the art. Moreover, the time scale of this process can further be reduced upto 5 ps (~200 GHz) by increasing the thermal conductivity of the substrate and decreasing the sample size to minimize the lateral diffusion time. Further, the FM layer with a higher spin switching threshold energy can be adapted to demonstrate the efficient ultrafast photo-thermal effect and switching of terahertz spin current.

### 3. Conclusion

In summary, we demonstrated an ultrafast photo-thermal switching of the transient terahertz spin current that manifests as the phase reversal of the emitted terahertz light. The experiment provides insight into the ultrafast heat transfer process in the spintronic system, which was otherwise assumed to have a negligible impact on terahertz spintronic emitters. The thermal energy provided by the ultra-short light pulse manipulates the anisotropy energy barrier height of ferromagnets resulting in the switching of the spin polarization. Moreover, the results indicate that the photo-thermal effect is mainly dominated by a single laser pulse. Our findings

provide a route to develop an on-chip scalable array of spintronics devices with unique ultrafast writing and readout channels, which allows material selectivity from a broad class of ferromagnetic materials. The higher-order reconfiguration channels, such as electric field, spatial, and strain control of magnetic anisotropy, can further enable control of spin polarization by tailoring the magnetic energy barrier. Thus, the photo-thermal switching of terahertz spin current has a strong potential to enable the read and write processes in the spintronics devices at terahertz speeds for future ultrafast computing and communication technologies.

#### **4. Methods**

*Sample preparation:* For a comprehensive comparison, three samples (NiFe/Pt, NiFe/W, and W/ NiFe/Pt) (refer Supplementary Section S1) were sputtered on Quartz substrate at 1 mTorr argon pressure at 10-Watt DC power. A protective capping layer of 10 nm Al<sub>2</sub>O<sub>3</sub> was deposited on all samples. The substrates were chosen from the same batch to avoid any fluctuation in the terahertz pulse due to the variation in substrate thickness. We first statistically characterize the sample quality by investigating the terahertz emission from the two bilayers, which adds upto the emission from the trilayer, proving the excellent quality and consistent results of the sample (refer Supplementary Section S1). In addition to it, the VSM measurements were performed to ascertain the coherent magnetic properties of the bilayer and trilayer samples. AFM (Atomic Force Microscopy) (refer Supplementary Section S5) was used to check the surface uniformity of the deposited thin film stacks.

*Terahertz Measurements:* The emission from the spintronic emitter was detected using a ZnTe nonlinear crystal. An optical laser beam (800 nm and 1.55 eV) of 35 fs pulse width with a 1kHz repetition rate was used. As a standard technique, it is split into two beams where one is used as a pump laser to illuminate the spintronic terahertz emitter, and the other is guided through

the delay stage to be used as a time-matched probe on the detector. The terahertz induces birefringence in the detector ZnTe crystal, and thus the probe laser experiences a change in the polarization, which is proportional to the transient terahertz electric field value. Thereafter a combination of quarter waveplate and Wollaston prism is used to split the probe laser in  $s$  and  $p$  polarization. A balanced photodiode provides the measure of the change in laser polarization. Thus, by using the electro-optic sampling, the complete terahertz pulse is mapped in time-domain. The optical beam is 7 mm in diameter. To record the THz-H hysteresis loop, the peak value of the terahertz pulse was recorded while sweeping the magnetic field. (refer Supplementary Section S2)

*Dual-beam terahertz setup and measurement:* For this experiment, the spintronic terahertz emitter is illuminated by two laser beams with a relative pulse delay of  $\sim 1.3$  ns (see Figure 4(a)). The fluences of these two laser pulses were carefully chosen from the region I and region II of the coercivity data (Figure 1(d)).

*Ultrafast reflectivity measurements:* Two laser beam of 800nm pump and probe is used in time-matched conditions to illuminate the system. The pump laser illuminates the sample at normal incidence while a low power probe laser illuminates the sample at roughly 15 degrees. The reflected probe intensity is recorded by changing the time delay between the probe and the pump laser. Each pump laser pulse irradiates the sample, which is spontaneously absorbed by the electrons/spins, leading to an increase in electronic temperature. Consequently, its absorption coefficient decreases and an additional laser used as a probe detects the change in reflected intensity. Later, the temperature falls when electronic angular momentum is transferred to the lattice, and after electron-phonon thermalization, heat diffuse laterally in the sample and, thereafter, thermalize with the environment to return to the initial state. Thus the exchange in energy at different stages (Figure 3(b)) explains the rise and fall of temperatures

of electrons ( $T_e$ ) and lattice ( $T_{ph}$ ), which is respectively governed by its specific heat. This behaviour is explained by the coupled two temperature (2T) model (refer Supplementary Section S3).

**Supporting Information**

Supporting Information is available from the Wiley Online Library or from the author.

**Acknowledgements**

The authors acknowledge research funding support from the Singapore Ministry of Education Academic Research Fund Grant Nos. MOE2017-T2-1-110 and MOE2016-T3-1-006(S). RM and RSR would like to acknowledge the National Research Foundation, Singapore, for support through NRF-CRP21-2018-003.

Received: ((will be filled in by the editorial staff))

Revised: ((will be filled in by the editorial staff))

Published online: ((will be filled in by the editorial staff))

## References

- [1] E. Beaurepaire, J.-C. Merle, A. Daunois, J.-Y. Bigot, *Physical Review Letters* **1996**, *76*, 4250.
- [2] M. Asada, S. Suzuki, *J Infrared Milli Terahz Waves* **2016**, *37*, 1185.
- [3] K. Cong, W. Jiang, B. E. Anthonio, G. T. Noe, H. Liu, H. Kataura, M. Kira, J. Kono, *ACS Photonics* **2020**, *7*, 1382.
- [4] B. Dieny, I. L. Prejbeanu, K. Garelo, P. Gambardella, P. Freitas, R. Lehndorff, W. Raberg, U. Ebels, S. O. Demokritov, J. Akerman, A. Deac, P. Pirro, C. Adelman, A. Anane, A. V. Chumak, A. Hirohata, S. Mangin, S. O. Valenzuela, M. C. Onbaşlı, M. d'Aquino, G. Prenat, G. Finocchio, L. Lopez-Diaz, R. Chantrell, O. Chubykalo-Fesenko, P. Bortolotti, *Nat Electron* **2020**, *3*, 446.
- [5] E. Beaurepaire, G. M. Turner, S. M. Harrel, M. C. Beard, J.-Y. Bigot, C. A. Schmuttenmaer, *Appl. Phys. Lett.* **2004**, *84*, 3465.
- [6] K. Sengupta, T. Nagatsuma, D. M. Mittleman, *Nature Electronics* **2018**, *1*, 622.
- [7] M. Tonouchi, *Nature Photonics* **2007**, *1*, 97.
- [8] T. Nagatsuma, G. Ducournau, C. C. Renaud, *Nature Photonics* **2016**, *10*, 371.
- [9] P. H. Siegel, *IEEE Transactions on Microwave Theory and Techniques* **2004**, *52*, 2438.
- [10] K. Ajito, Y. Ueno, *IEEE Transactions on Terahertz Science and Technology* **2011**, *1*, 293.
- [11] T. Kampfrath, M. Battiato, P. Maldonado, G. Eilers, J. Nötzold, S. Mährlein, V. Zbarsky, F. Freimuth, Y. Mokrousov, S. Blügel, M. Wolf, I. Radu, P. M. Oppeneer, M. Münzenberg, *Nature Nanotechnology* **2013**, *8*, 256.
- [12] T. Seifert, S. Jaiswal, U. Martens, J. Hanneegan, L. Braun, P. Maldonado, F. Freimuth, A. Kronenberg, J. Henrizi, I. Radu, E. Beaurepaire, Y. Mokrousov, P. M. Oppeneer, M.

- Jourdan, G. Jakob, D. Turchinovich, L. M. Hayden, M. Wolf, M. Münzenberg, M. Kläui, T. Kampfrath, *Nature Photonics* **2016**, *10*, 483.
- [13] J.-Y. Bigot, M. Vomir, E. Beaurepaire, *Nature Physics* **2009**, *5*, 515.
- [14] A. V. Kimel, M. Li, *Nat Rev Mater* **2019**, *4*, 189.
- [15] L. Cheng, X. Wang, W. Yang, J. Chai, M. Yang, M. Chen, Y. Wu, X. Chen, D. Chi, K. E. J. Goh, J.-X. Zhu, H. Sun, S. Wang, J. C. W. Song, M. Battiato, H. Yang, E. E. M. Chia, *Nat. Phys.* **2019**, *15*, 347.
- [16] Z. Jin, A. Tkach, F. Casper, V. Spetter, H. Grimm, A. Thomas, T. Kampfrath, M. Bonn, M. Kläui, D. Turchinovich, *Nature Phys* **2015**, *11*, 761.
- [17] V. P. Zhukov, E. V. Chulkov, P. M. Echenique, *Phys. Rev. B* **2006**, *73*, 125105.
- [18] M. Battiato, K. Carva, P. M. Oppeneer, *Physical Review Letters* **2010**, *105*, 027203.
- [19] M. Battiato, K. Carva, P. M. Oppeneer, *Phys. Rev. B* **2012**, *86*, 024404.
- [20] M. Battiato, P. Maldonado, P. M. Oppeneer, *Journal of Applied Physics* **2014**, *115*, 172611.
- [21] D. Kong, X. Wu, B. Wang, T. Nie, M. Xiao, C. Pandey, Y. Gao, L. Wen, W. Zhao, C. Ruan, J. Miao, Y. Li, L. Wang, *Advanced Optical Materials* **n.d.**, *7*, 1900487.
- [22] A. Shorrock, M. T. Hibberd, T. Thomson, P. W. Nutter, D. M. Graham, in *2019 44th International Conference on Infrared, Millimeter, and Terahertz Waves (IRMMW-THz)*, **2019**, pp. 1–1.
- [23] M. Chen, Y. Wu, Y. Liu, K. Lee, X. Qiu, P. He, J. Yu, H. Yang, *Advanced Optical Materials* **2019**, *7*, 1801608.
- [24] A. Deka, B. Rana, R. Anami, K. Miura, H. Takahashi, Y. Otani, Y. Fukuma, *Phys. Rev. B* **2020**, *101*, 174405.



- [25] T. J. Huisman, R. V. Mikhaylovskiy, J. D. Costa, F. Freimuth, E. Paz, J. Ventura, P. P. Freitas, S. Blügel, Y. Mokrousov, Th. Rasing, A. V. Kimel, *Nature Nanotechnology* **2016**, *11*, 455.
- [26] M. B. Jungfleisch, Q. Zhang, W. Zhang, J. E. Pearson, R. D. Schaller, H. Wen, A. Hoffmann, *Phys. Rev. Lett.* **2018**, *120*, 207207.
- [27] M. Tong, Y. Hu, Z. Wang, T. Zhou, X. Xie, X. Cheng, T. Jiang, *Nano Lett.* **2021**, *21*, 60.
- [28] C. Zhou, Y. P. Liu, Z. Wang, S. J. Ma, M. W. Jia, R. Q. Wu, L. Zhou, W. Zhang, M. K. Liu, Y. Z. Wu, J. Qi, *Phys. Rev. Lett.* **2018**, *121*, 086801.
- [29] Q. Zhang, D. Hong, C. Liu, R. Schaller, D. Fong, A. Bhattacharya, H. Wen, in *2019 Conference on Lasers and Electro-Optics (CLEO)*, **2019**, pp. 1–2.
- [30] X. Wang, L. Cheng, D. Zhu, Y. Wu, M. Chen, Y. Wang, D. Zhao, C. B. Boothroyd, Y. M. Lam, J.-X. Zhu, M. Battiato, J. C. W. Song, H. Yang, E. E. M. Chia, *Advanced Materials* **2018**, 1802356.
- [31] X. Chen, X. Wu, S. Shan, F. Guo, D. Kong, C. Wang, T. Nie, C. Pandey, L. Wen, W. Zhao, C. Ruan, J. Miao, Y. Li, L. Wang, *Appl. Phys. Lett.* **2019**, *115*, 221104.
- [32] T. Seifert, U. Martens, S. Günther, M. A. W. Schoen, F. Radu, X. Z. Chen, I. Lucas, R. Ramos, M. H. Aguirre, P. A. Algarabel, A. Anadón, H. S. Körner, J. Walowski, C. Back, M. R. Ibarra, L. Morellón, E. Saitoh, M. Wolf, C. Song, K. Uchida, M. Münzenberg, I. Radu, T. Kampftrath, *SPIN* **2017**, *07*, 1740010.
- [33] M. Venkatesh, S. Ramakanth, A. K. Chaudhary, K. C. J. Raju, *Opt. Mater. Express* **2016**, *6*, 2342.
- [34] J. de Vries, T. Bolhuis, L. Abelman, *New J. Phys.* **2017**, *19*, 093019.
- [35] R. Medwal, S. Gautam, S. Gupta, K. H. Chae, K. Asokan, G. R. Deen, R. S. Rawat, R. S. Katiyar, S. Annapoorni, *IEEE Magnetism Letters* **2018**, *9*, 1.

- [36] U. Atxitia, O. Chubykalo-Fesenko, J. Walowski, A. Mann, M. Münzenberg, *Phys. Rev. B* **2010**, *81*, 174401.
- [37] J. Hohlfeld, S.-S. Wellershoff, J. GÜdde, U. Conrad, V. Jähnke, E. Matthias, *Chemical Physics* **2000**, *251*, 237.
- [38] J. Mendil, P. Nieves, O. Chubykalo-Fesenko, J. Walowski, T. Santos, S. Pisana, M. Münzenberg, *Sci Rep* **2015**, *4*, 3980.

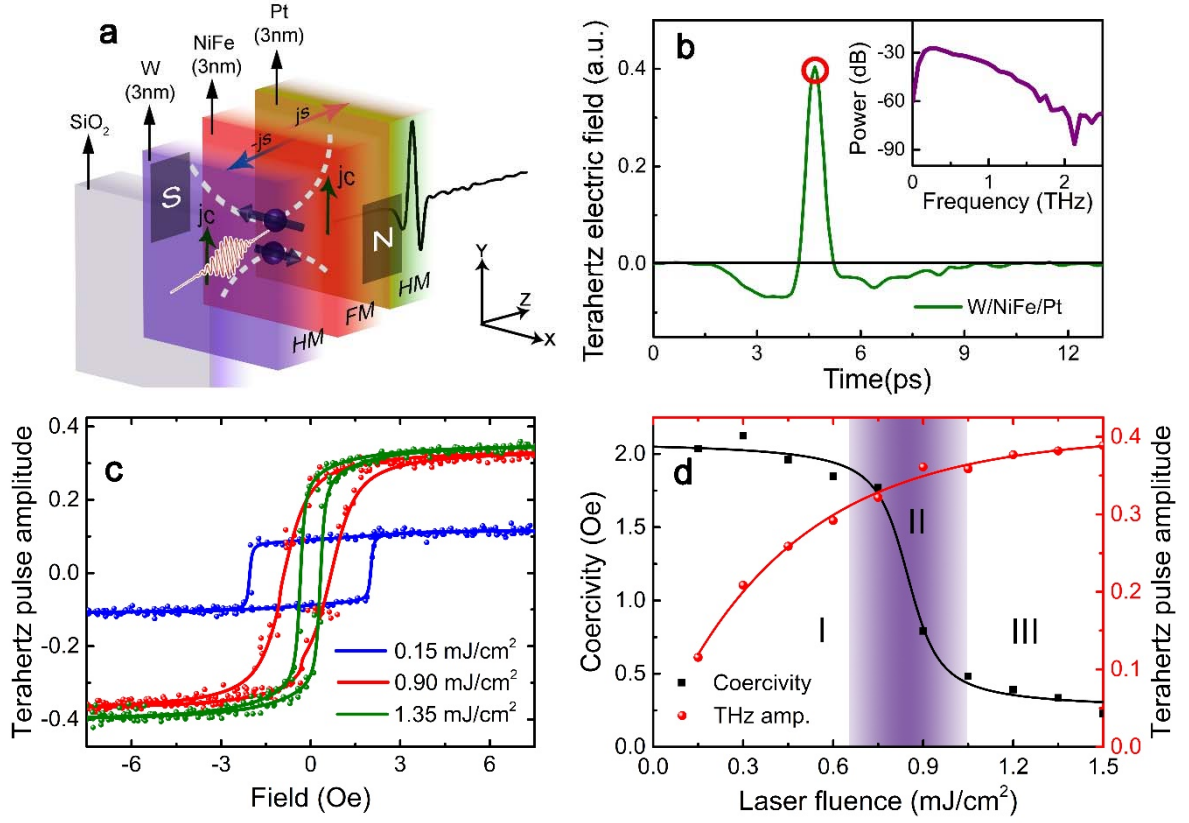


**Figure 1: Hysteresis loop formed by emitted terahertz fields.** (a) Schematic representation of terahertz emission from a trilayer W/NiFe/Pt structure. The femtosecond pulse leads to an ultrafast superdiffusion of spins in the adjacent HM layers, where it experiences an inverse spin Hall effect (ISHE) to produce transverse charge current and terahertz emission. (b) Electro-optic signal of terahertz pulses obtained from W/NiFe/Pt thin films. The peak of the emitted terahertz pulse (marked with a red circle) is continuously recorded while varying the magnetic field to measure the THz-H hysteresis loop. Inset: fast Fourier transform of the electro-optic signal. (c) The amplitude of the emitted terahertz pulse as a function of the magnetic field (THz-H hysteresis loop) for three fluences 0.15 mJ/cm<sup>2</sup>, 0.90 mJ/cm<sup>2</sup>, and 1.35 mJ/cm<sup>2</sup>. The solid line indicates the Langevin fits (d) Coercive field and amplitude of emitted terahertz pulse as a function of pump laser fluence.

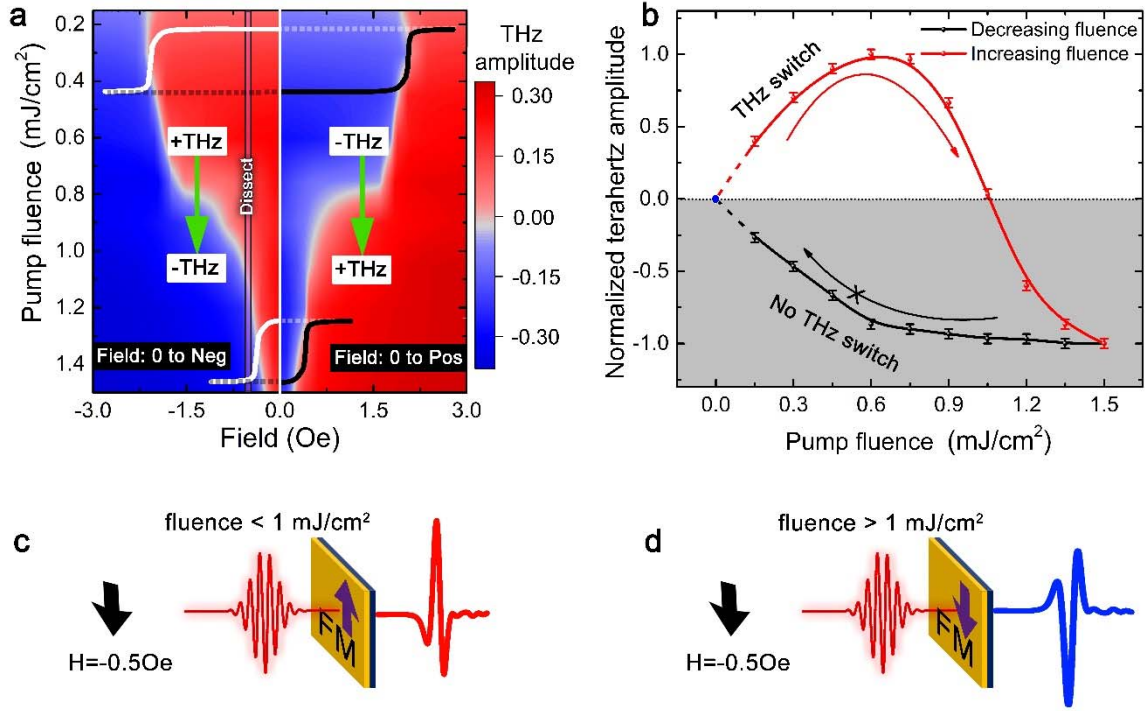


**Figure 2: Photo-thermal switching of spin enabled reconfigurable terahertz spintronic emission from W/NiFe/Pt.** (a) 3D map of THz-H hysteresis loop as a function of pump laser fluence for given magnetic fields. The green arrow indicates the terahertz phase reversal with laser fluence in a particular range of magnetic fields between 0.2 Oe to 2.1 Oe. (b) Terahertz phase reversal with increasing fluence at -0.5 Oe (along the dissect line). The terahertz amplitude reaches the maximum at the fluence of 0.60 mJ/cm² due to increasing spin current density and experiences phase reversal for fluence larger than 1 mJ/cm². Schematic showing the effect of the fluence on the phase reversal of emitted terahertz for (c) fluence < 1 mJ/cm² and (d) fluence > 1 mJ/cm².

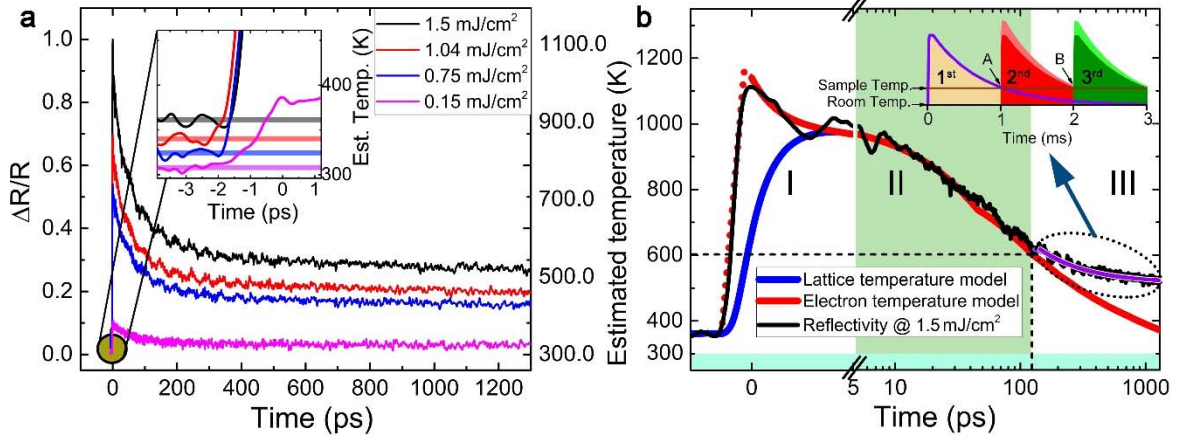


**Figure 3: Ultrafast temperature dynamics of W/NiFe/Pt.** (a) Time-resolved electro-optic signal of ultrafast reflectivity data, highlighting the electron temperature after excitation. Inset: electron temperature before excitation. This demonstrates the remnant heat in the sample from the previous laser pulse (b) Estimated temperature of trilayer heterostructure (from reflectivity data) as a function of time, with 2T (2-Temperature) model, used to estimate the temperature dynamics (refer Supplementary Section S3); Region I: electrons absorb the laser and spontaneously rise in temperature (dotted red). Consequently, the electronic temperature thermalizes with the phonons (phonon temperature shown in blue), Region II: Heat from electrons and phonons together diffuse laterally in the entire metallic heterostructure. Region III: The trilayer exchange energy with the environment through heat diffusion across the substrate to thermalize with room temperature. The experimental data deviate from the model since the slow thermalization with the environment was not accounted for in the 2T model. This exponential relaxation (purple line) is artistically shown in the inset. Note that the 1<sup>st</sup> control pulse leads to significant remnants at 1<sup>st</sup> readout (denoted by A) (~20%) and close to zero remnants at 2<sup>nd</sup> readout (denoted by B) (~4%).

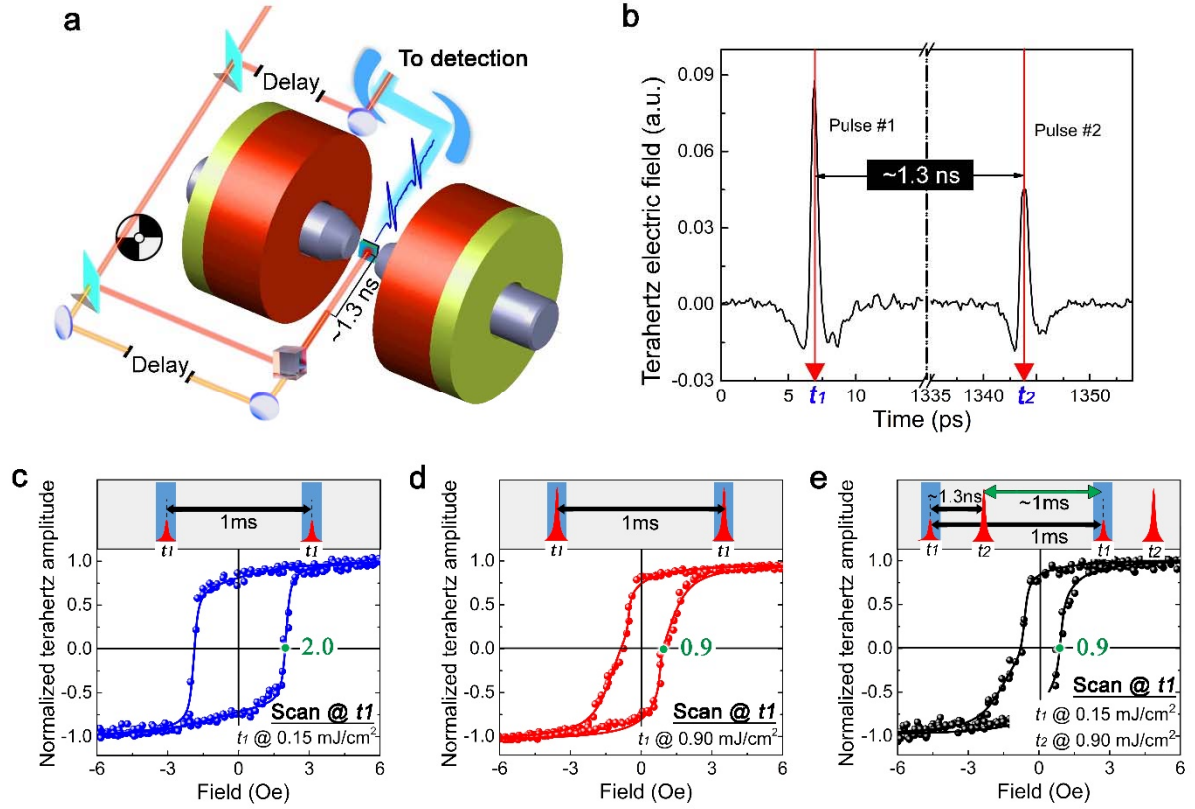


**Figure 4: Single laser pulse dominated ultrafast photo-thermal switching** (a) Schematic of the setup used to generate terahertz emission using two laser pulses temporally separated by  $\sim 1.3$  ns (b) Dual terahertz emission correspond to the two laser pulses #1 and #2 at temporal positions  $t_1$  and  $t_2 = (t_1 + 1.3 \text{ ns})$  respectively. (c) THz-H hysteresis loop for laser fluence of  $0.15 \text{ mJ/cm}^2$  at time instance  $t_1$  (d) THz-H hysteresis loop for laser fluence of  $0.90 \text{ mJ/cm}^2$  at temporal instance  $t_1$  (e) THz-H hysteresis loop scanned at time instance  $t_1$  when the sample is excited with both pulses located at time instances of  $t_1$  and  $t_2$  with fluences of  $0.15 \text{ mJ/cm}^2$  and  $0.90 \text{ mJ/cm}^2$ , respectively.